Optics and Laser Technology 108 (2018) 521–528

Contents lists available at ScienceDirect

Optics and Laser Technology

journal homepage: www.elsevier.com/locate/optlastec

Full length article

Ti6Al4V lightweight lattice structures manufactured by laser powder bed fusion for load-bearing applications

Anton du Plessis [a,b,*], Ina Yadroitsava [c], Igor Yadroitsev [c]

[a] CT Scanner Facility, Stellenbosch University, Stellenbosch 7602, South Africa
[b] Physics Department, Stellenbosch University, Stellenbosch 7602, South Africa
[c] Department of Mechanical and Mechatronic Engineering, Central University of Technology, Free State, Bloemfontein 9300, South Africa

ARTICLE INFO

Article history:
Received 14 May 2018
Received in revised form 11 July 2018
Accepted 19 July 2018
Available online 29 July 2018

Keywords:
Additive manufacturing
Laser powder bed fusion
Lattice structure
MicroCT
Simulation
Compressive strength

ABSTRACT

Additively manufactured (AM) lattice structures allow complex-shaped and custom parts, with superior design that cannot be produced by traditional methods. For medical implants, AM lattice structures are aimed at matching the elastic modulus of bone while providing strength and allowing bone in-growth for long-term stability. In this study, relatively thick struts are investigated in an attempt to match the properties of cortical bone, which is meant for the internal structural integrity of the implant, while a smaller lattice may be used for near-surface parts of an implant. In this work we investigate additively manufactured lattice samples produced by Laser Powder Bed Fusion (LPBF) of Ti6Al4V ELI, with samples having approximately 50% regular porosity. In particular, we experimentally compare two designs: diagonal and rhombic. MicroCT-based static loading simulations are used to highlight stress hotspots in the two designs, to highlight possible failure locations. Physical compression testing to initial failure and subsequent microCT highlight the locations of initial failure, which correlate well with the simulation stress hotspots. Both designs show excellent strength (120–140 kN failure load) and effective compressive elastic modulus corresponding well to simulations. Differences between microCT-based simulations of the produced lattices and those of ideal design parameters can be attributed mainly to surface roughness, and slightly thinner manufactured struts of the as-built lattices, with similar trends for the two model designs. These results validate experimentally that both designs are suitable for load-bearing applications.

1. Introduction

The advantages of additive manufacturing (AM) are the reduction of the time from the concept of the part to its production, reducing the material, the flexibility and freedom of design, multi-materials, gradient-structures and composites in a single cycle, the production of unique alloys/compositions and the simultaneous production of functional parts [1,2]. Products fabricated through laser-based AM processes are used in the medical field, dentistry, aerospace, automotive and power industries, to name only a few. Despite the high degree of complexity possible by Laser Powder Bed Fusion (LPBF), some limitations exist – in particular for overhanging structures, and hence the size and shape of the deliberate pore spaces in cellular structures are limited [1]. These limitations are caused by the track-by-track, layer-by-layer nature of LPBF. Fast heating/melting/cooling in LPBF leading to non-equilibrium metallurgical process cause significant differences in mechanical properties of the LPBF objects in comparison with traditional casting and forged parts [3]. Further studying the microstructure, physical, mechanical properties and heat treatments of AM parts to compile high quality requirements for high-specification components is a relevant and important task for the greater use of the relatively new AM technologies by industry [1,2,4]. Obtaining lightweight structures with mechanical properties close to the properties of bones is another important task for the widespread adoption of LPBF for biomedical applications such as customized implants or in the aerospace field, where strength, reliability and low weight are the most important issues [5,6].

Additive manufacturing of Ti alloys has been the topic of investigation of numerous researchers over the last few years [7]. Ti6Al4V is one of the principal biomaterials for implants but its properties are far from human bones: Ti6Al4V alloy has a density of 4.43 g/cm^3, which is twice heavier than cortical bone (1.99 g/cm^3). Ultimate tensile and compression strengths and the elastic modulus are all higher in Ti6Al4V alloy by more than 5–7 times in comparison with hard bone tissues. By producing a metal

* Corresponding author at: CT Scanner Facility, Stellenbosch University, Stellenbosch 7602, South Africa.
E-mail address: anton2@sun.ac.za (A. du Plessis).

https://doi.org/10.1016/j.optlastec.2018.07.050
0030-3992/

lattice structure by LPBF, the mechanical properties of the metal lattice can be approximated to the properties of bones [8,9]. The production of latticed Ti6Al4V structures by additive manufacturing has been reviewed recently by Tan et al. [10] who mention that among the many lattice designs, not only one ideal solution exists for any specific task and there may be many optimal solutions (i.e. lattice designs). However, there is still a need for additional analysis of AM lattice structure designs to validate their physical compressive strength when produced by additive manufacturing because its mechanical performance depends on the manufacturing strategy and process parameters [3,11,12].

In this work, LPBF lattice structures of two designs were tested. This testing involved non-destructive microCT analysis before compression, physical compression testing and microCT analysis after compression, as well as optical microscopy. MicroCT allows inspection for presence of defects such as internal porosity in the struts, for surface roughness and CAD model deviations. Static load simulations were conducted on the lattice structures (using the CAD data) to analyze the maximum Von Mises stress distributions and compare these between two designs. A microCT-based load simulation was also applied to the two LPBF samples of different design types and compared to their ideal stress distributions. In this way the differences could be analyzed and the effect of build imperfections can be related directly to the mechanical properties, found by physical compression testing. MicroCT analysis of compressed lattices also highlight locations of failure, correlating to the stress regions found by simulation. The lattices tested here were designed with 50% density and large unit cells resulting in strut thickness values >1.5 mm. The aim was to match the properties of cortical bone, and provide an analysis of lattices meant for load-bearing applications. The lattice density is expected to affect the effective elastic modulus irrespective of the strut thickness (determined by the unit cell size selected). The thicker struts are selected to ensure accurate manufacturing and less effect of manufacturing imperfections, compared to lattices with thin struts. The two designs were selected based on their availability in software tools, their relatively simple design and both are applicable to bone implants.

2. Materials and methods

12 cubes with periodic cellular lattice structures $25 \times 25 \times 25\ \mathrm{mm}^3$ and solid top and bottom layers of 1 mm in thickness (Fig. 1) were produced by an EOSINT M280 system. Samples were fabricated at standard process parameters recommended by EOS for Ti6Al4V at 30 μm powder layer thickness. Argon was used as the protective atmosphere; the oxygen level in the chamber was controlled in the range of 0.07–0.12%. The chemical composition of the spherical gas-atomized Ti6Al4V (ELI) (−45 μm) powder from TLS Technik is given in Table 1. The 10th, 50th and 90th percentiles of equivalent diameter (weighted by volume) of the powder particles were d_{10} = 13 μm, d_{50} = 23 μm and d_{90} = 37 μm.

Rhombic and diagonal lattice structures were designed with a target 50% volume fraction (Fig. 1). In this case, the target volume fraction and large unit cell size with relatively thick struts are investigated in an attempt to match the properties of cortical bone,

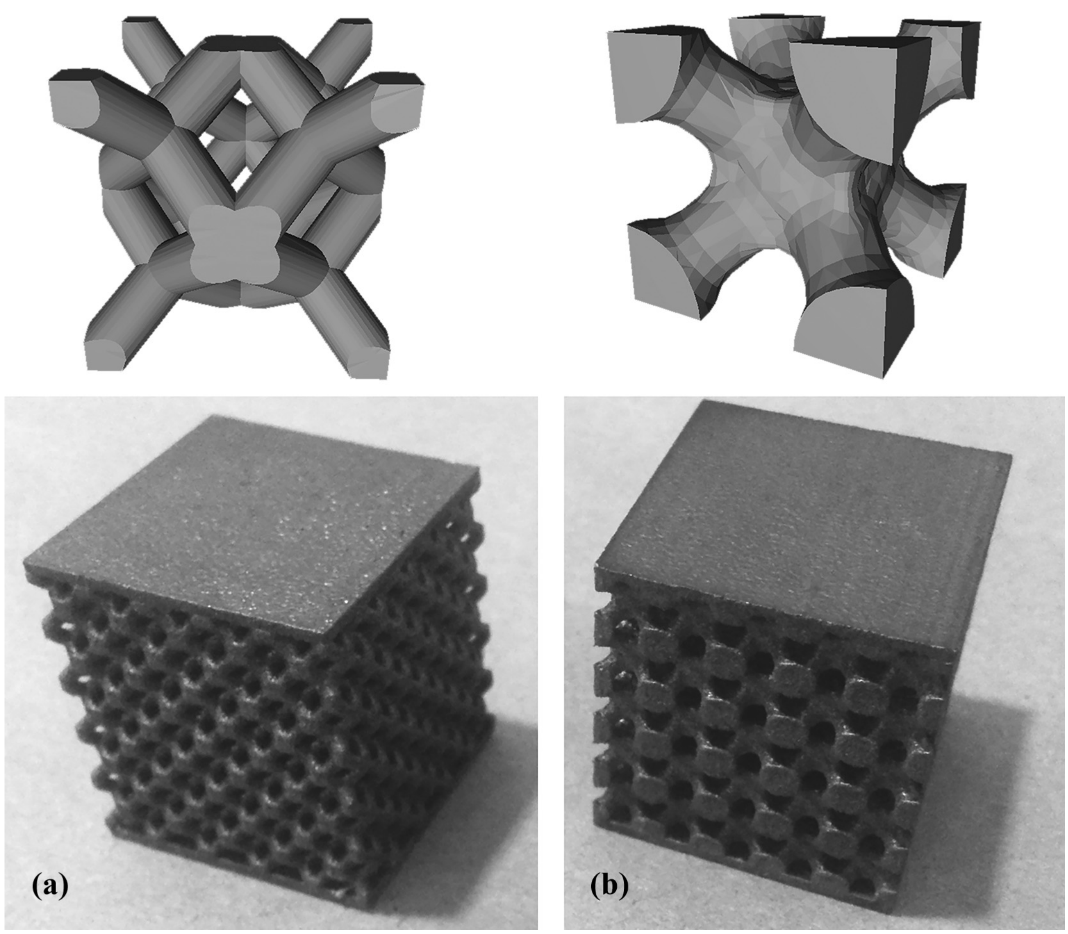

Fig. 1. CAD models of unit cells and LPBF tessellated lattice parts with rhombic (a) and diagonal designs (b).

Table 1
Chemical composition of powder (in wt.%).

Ti	Al	V	O	N	H	Fe	C	Y
Bal.	6.34	3.94	0.058	<0.006	0.001	0.25	0.006	<0.001

which is meant for the internal structural integrity of the implant. A fixed unit cell size of 5 mm was selected. The resulting maximum strut diameters were 1317 μm for rhombic structures and 1669 μm for diagonal types of the unit cells, measured using the maximum-spheres method (wall thickness analysis function in VGStudioMax 3.0).

Before cutting from the baseplate, specimens were heat treated for 3 h in Ar atmosphere at 650 °C for stress relieving. Mechanical properties of LPBF specimens were obtained through uniaxial compression tests. Compressive stress was calculated as ratio of load (N) over the top surface area (25 × 25 mm) in direct contact during compression tests. Compression tests were carried out with an Amsler testing machine. The total deformation was measured using a digital image correlation setup. The baseplate was tracked to measure total deformation up to full densification, after which the test was stopped. Two initial samples were compressed to initial failure (first yielding) on a different system, and used for detailed imaging of the first failure location using microCT. Initial failure refers here to the first point of fracture at the initial peak stress value, after which there follows a stress plateau prior to final densification – this is typical for cellular materials.

The samples were individually scanned before and after compressive testing to failure, using 180 kV and 160 μA, at 30 μm voxel size. At this voxel size the cylindrical scan volume is approximately 60 mm high and wide. Other settings included 1 mm copper beam filtration, acquisition time of 333 ms per image, with averaging of 2 images and skipping of 1 image at each step position, with 3000 step positions used to record images in one full rotation of the sample. Reconstruction was performed using a moderate beam hardening correction factor. Scans were performed on a General Electric VTomeX L240 system. MicroCT data was visualized and analysed in Volume Graphics VGStudioMax 3.0. Analysis of porosity and CAD variance analysis for additive manufactured medical implants was described before by du Plessis *et al.* [13,14].

A structural mechanics simulation was performed on the CAD data and the actual microCT data. The simulation on the CAD (stl) data ("ideal" sample) was performed by creating an artificial voxel data set from the STL data, using the procedure "*convert to volume*". Structural mechanics simulation was performed using the method described in du Plessis *et al.* [15] and Broeckhoven *et al.* [16], using as inputs a Young's modulus of 115 GPa and 0.35 Poisson's ratio for Ti6Al4V, making use of the top and bottom of the sample as fixed and load regions. A nominal load value of 1 kN was applied to the top of the sample in the simulation in order to compare maximum Von Mises stress between different samples. Only linear elastic simulations were used here to highlight the weakpoints in the structure which lead to initial yielding. The maximum Von Mises stress values are obtained by statistically analysing the Von Mises stress across the entire structure and using the top 1% as a "maximum" value. This is in no way meant to correlate directly to traditional stress, and is meant only to compare samples for local stress hotspot generation, which can affect the mechanical response. Recently, microCT data was used for similar simulation efforts for single cell lattices in [17], where deformation was followed by simulation. Our simulations differ in that only the simplest linear elastic simulation of the original form is used, prior to deformation. In another similar study, high stress values in microCT-based simulations of lattices could be correlated to failure locations – mainly attributed to poor build quality in the thin struts carrying most load [18].

3. Results and discussion

3.1. Morphological and microstructural analysis of LPBF lattice cubes

MicroCT data before physical compression showed a lack of internal porosity in the struts, with values similar to that found in a previous study using this LPBF system with the same process parameters [19]. The rhombic structure had a total porosity (in struts) of 0.00136% and the diagonal structure had 0.00429%. Both of these are negligibly small and are not expected to affect the mechanical properties of the samples. In order to visualize deviations of the parts compared to their design, a CAD variance analysis was applied. Under the chosen building and scanning strategies, the deviations from CAD design was very small: statistical analysis of the deviations across all surface points in the microCT data showed that both LPBF sample types were produced slightly smaller than their CAD design by 62 μm and 38 μm on average for the rhombic and diagonal designs respectively. The statistical distributions are shown in Fig. 2. Some additional material was present at places, especially in the diagonal type, at the underside of horizontal struts. This is also observed in the statistical distribution with an asymmetric profile for the diagonal type. This additional material found by microCT scans were only present in some places and were not found in regions of high stress (see simulations in next section), so was not expected to affect the mechanical properties.

More detailed morphogical analysis was applied from microCT data of all samples subjected to compression testing. Once the lattice region was selected (without top and bottom plates), the morphological analysis was applied in order to quantify the build quality and reproducibility and compare it to the design values. The morphological results are summarized in Fig. 3 and error bars are not included as the values are essentially identical across all 5 samples of each type (standard deviation in all values less than 0.1%). The morphological parameters reported here were proposed by Hildebrand and Rüegsegger [20] to describe the material volume fraction and the thickness of struts in 3D foam-like objects, especially bone. Since the lattice implants are meant to mimic bone structure, this type of analysis is very relevant. The most widely used measure is bone volume to total volume (*BV/TV*),

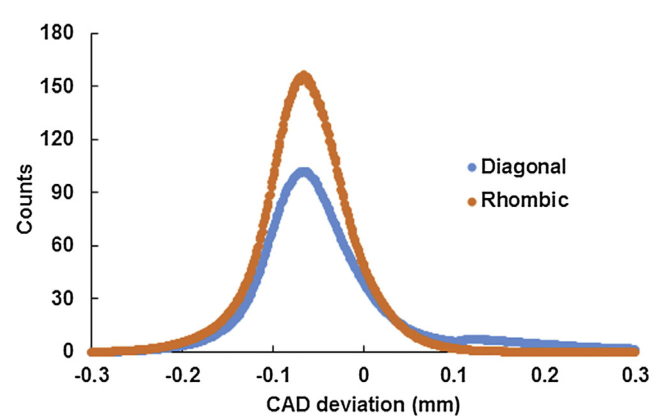

Fig. 2. CAD variance analysis for diagonal and rhombic LPBF samples with statistical distribution of variance data, indicating LPBF parts for both types were built slightly smaller than designed. This small value is considered acceptable since the single track width of the LPBF system is roughly 0.1 mm.

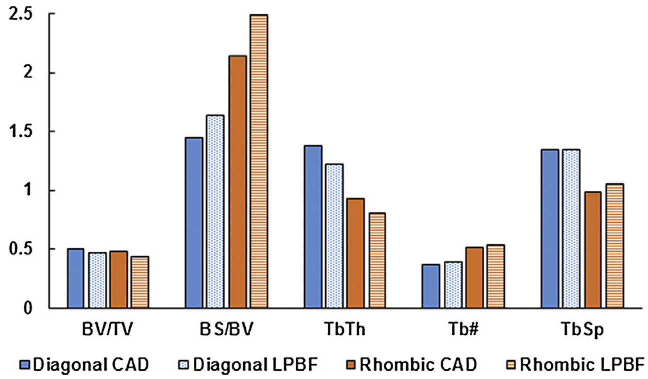

Fig. 3. Morphological analysis of prescribed CAD model and LPBF rhombic and diagonal structures received by microCT scans. The difference between CAD and actual models are affected by the larger surface area of the LPBF parts. The difference between diagonal and rhombic designs in general are mainly of interest here.

which is effectively the material volume fraction – in this work the design was aimed to be 50% BV/TV. Also included are the mean trabecular number *Tb#*, indicating the number of struts per unit length (mm) and the trabecular spacing *TbSp*, indicating the effective spacing between struts. These values are relatively easily obtained from microCT data and widely used in biomedical research, especially in studies of bones. A particularly useful value for additive manufactured parts is the *BS/BV* value which refers to the ratio of the material surface area (*BS*) to the material volume (*BV*). For a sample with higher surface roughness, of the same design, the value will be higher. For different designs, a higher value might be more conducive to cell growth due to the larger relative surface area available. The results in Fig. 4 show that the LPBF parts differ from their CAD design as they have a lower material volume fraction (as also seen from CAD variance analysis). The *BS/BV* values are higher as expected due to the surface roughness. It is interesting to note that the rhombic design has a significantly higher surface area per volume, which might have some advantages for cell growth when such a lattice is used in an implant. The trabecular thickness *TbTh* is lower in each case compared to its CAD design (also as expected from previous CAD variance analysis), and the trabecular thickness is lower in the rhombic design, indicating it has on average thinner struts. The mean trabecular number *Tb#* is higher in the rhombic design compared to diagonal, to compensate for its thinner struts while maintaining similar total volume fraction. Consequently, the trabecular spacing *TbSp* is also lower in the rhombic design, compared to diagonal.

As has been shown, the microstructure of as-built Ti6Al4V ELI alloy typically consists of α′ martensite [21,22]. The microstructures of the LPBF cellular structures are shown in Fig. 4. Prior β grains were oriented almost parallel to the building direction (Fig. 4b, d); at perpendicular cross-sections the grain boundaries also were well distinguished (Fig. 5a, c) similar to Ti6Al4V solid blocks manufactured in vertical direction at the same process-parameters and scanning strategy [19]. After a stress-relieving heat-treatment at 650 °C for 3 h, no significant changes in the microstructures have been found.

Attached powder particles and rough surfaces inside the cellular structures are visible in the cross-sections (Fig. 4). This surface roughness of produced samples is typical for LPBF and can be

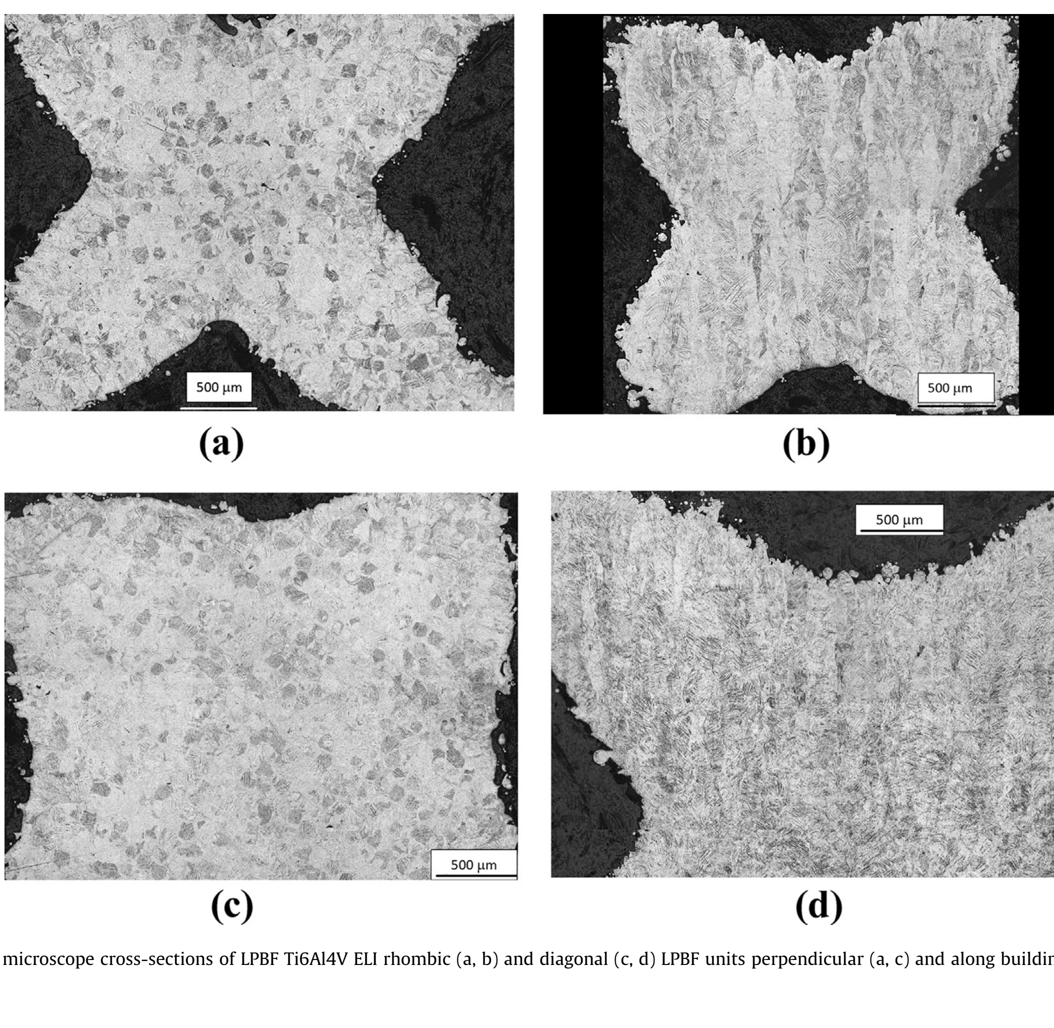

Fig. 4. Optical microscope cross-sections of LPBF Ti6Al4V ELI rhombic (a, b) and diagonal (c, d) LPBF units perpendicular (a, c) and along building direction (b, d).

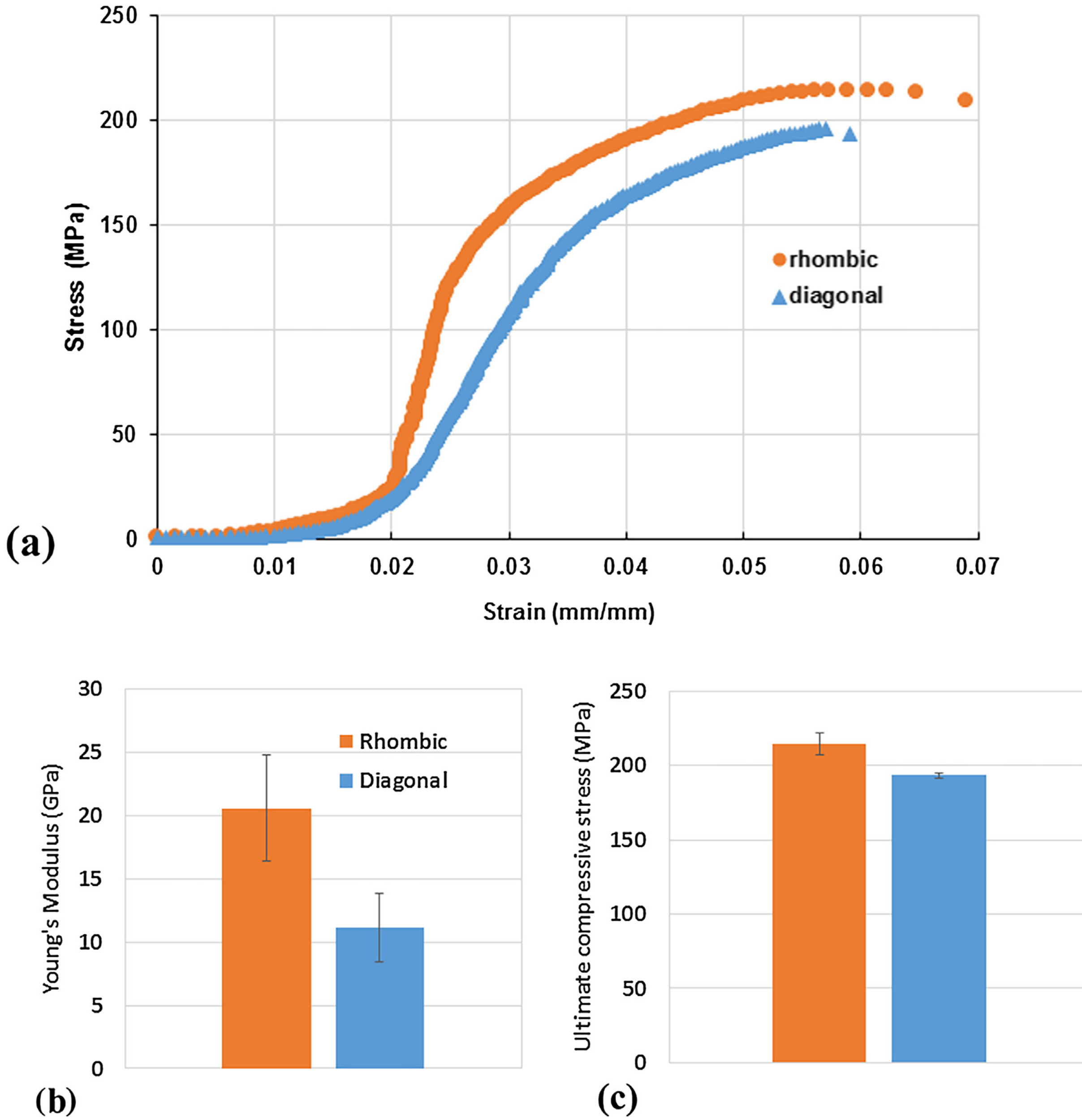

Fig. 5. Compression test results from 5 samples of each type: (a) one representative stress-strain curve of each type, (b) mean and standard deviation of effective compressive elastic modulus and (c) ultimate compressive stress values.

expected to affect the mechanical properties. Under compression testing, the loading direction was co-axed with building direction for both types of tested structures.

3.2. Mechanical testing of LPBF cubes

Mechanical compression tests of 10 samples were conducted to failure, with representative stress-strain curves of one sample of each shown in Fig. 5a. The effective compressive elastic modulus was calculated in the linear region 50–150 MPa, and the ultimate compressive stress was well confined in a small range around 200 MPa (~130 kN for this 25 mm sample). The results are summarized in Fig. 5b and c.

The effective compressive elastic modulus was lower for the diagonal-type, which also has a slightly lower ultimate compressive stress, indicating it is the weaker of the two structures. The ultimate compressive stress varies only within a small range, and corresponds to loads in the range of 190–225 MPa, for both types. It was noted that the crushing of bands of struts occur differently in the two designs. The crush band at 45° to the loading direction in the case of the rhombic design has been observed previously by Li *et al.* [23]. Crush bands perpendicular to the loading direction occurs in the diagonal design.

3.3. MicroCT-based simulations for LPBF cubes

MicroCT scans before and after physical compression of LPBF cellular structures were performed, with the aim to visualize failure locations and correlate these with stress distributions from simulations. MicroCT-based static load simulations show that the ideal rhombic-designed tessellated sample has a slightly lower maximum Von Mises stress, 29 MPa *versus* the 31 MPa of the diagonal design. The same trend is found for simulations on the actual produced sample data, i.e. max stress of 39 MPa *versus* 41 MPa and this trend corresponds to that found by mechanical tests (Fig. 5). The difference between Von Mises stress of the actual part (microCT simulation) and that of its design (CAD simulation) is significant and can be attributed mainly to surface roughness and slightly thinner struts than designed, increasing the Von Mises stress values.

MicroCT simulations indicate the location of the highest Von Mises stress located near the top and the bottom of the rhombic sample (Fig. 6a) in the strut junctions. Fig. 6c shows an overlay of the before and after compression showing the actual deformation with before-loading (gray) and after-loading (red colour). Fig. 7 shows microCT slice images of the simulation of stress distributions for loading and the corresponding failure cracks of the same location after compression (for the exact same slice). This confirms the good correlation between high stress values and failure locations in the rhombic sample. Fig. 7(b) presents orthogonal slice views of the failure location, near the top across the strut junctions: the thin black line is the initial failure crack, in the corner of the rhombic sample (red arrow). Similar results were found by Choy *et al.* [24] where during compression of LPBF cubic lattices the first collapse initiated from the layer at the edge or adjacent to the edge of samples.

The diagonal design shows large areas of high stress in the middle of the sample, compared to the edges, and first failure occurs in the middle of this sample as confirmed by significant cracking observed in microCT images of the middle of the sample shown in Fig. 7c, d. Interesting is that the highest localized stress values are found near the outside of the sample, but the failure occurs on the inside where larger high-stress areas are visible. This means that small localized stress hotspots are not the only important factor in determining failure location, but the size of the stress hotspot as well, at least for static loading.

The results obtained on the two lattice types are promising for future application of these designs in load-bearing applications. The microCT-based load simulation results could be correlated with failure locations, which also can assist in producing stronger parts by adding material at areas of high stress. The method will find particular use when analyzing more complex parts, especially when they are connected to solids or where they are truncated. In the case of the rhombic design, the failure occurred on the top at

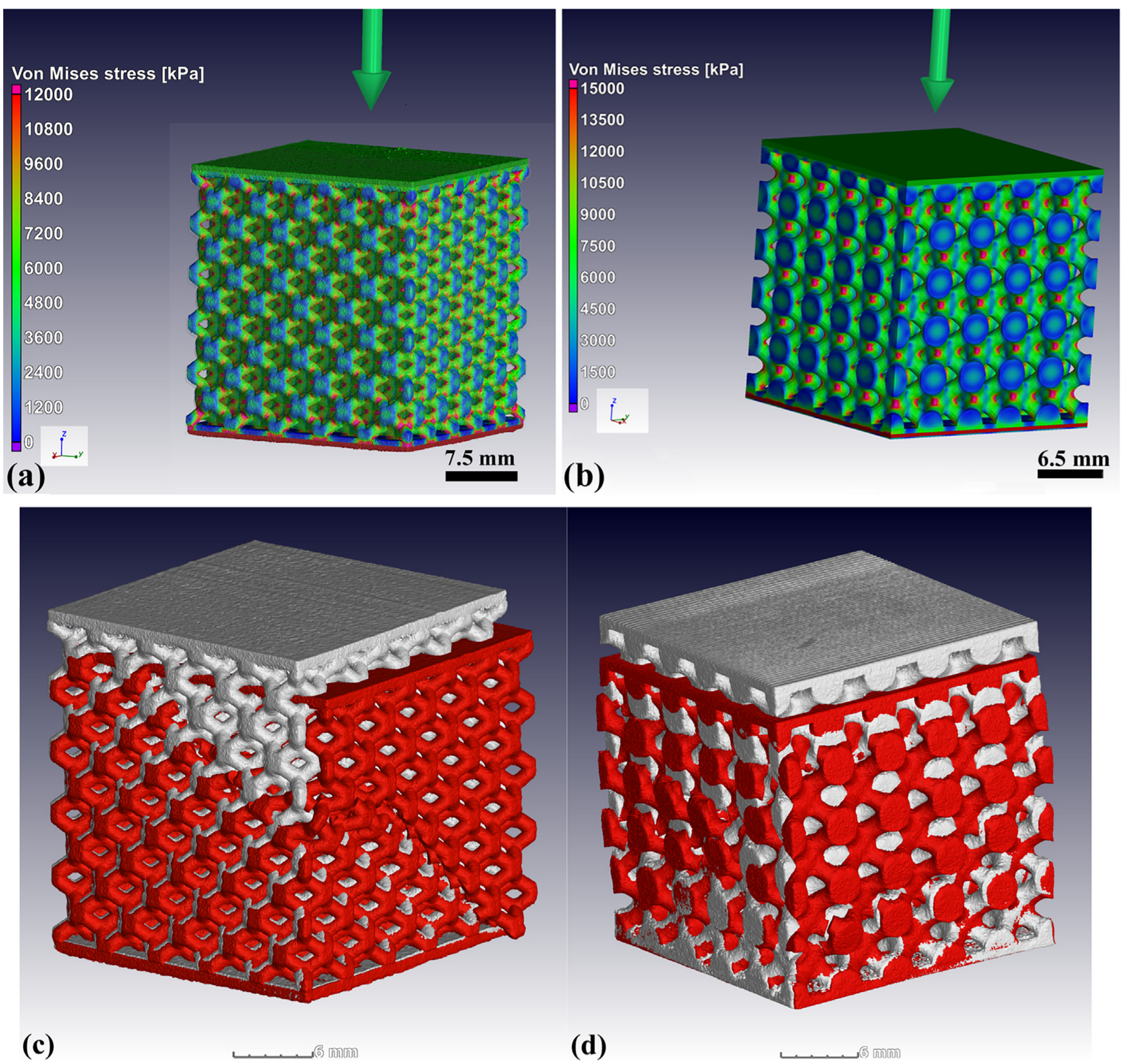

Fig. 6. MicroCT simulation of von Mises stress distributions in 3D samples under loading: (a) rhombic and (b) diagonal samples; overlay before and after compression showing the actual deformation of LPBF samples by red/orange colour for (c) rhombic and (d) diagonal samples. (For interpretation of the references to colour in this figure legend, the reader is referred to the web version of this article.)

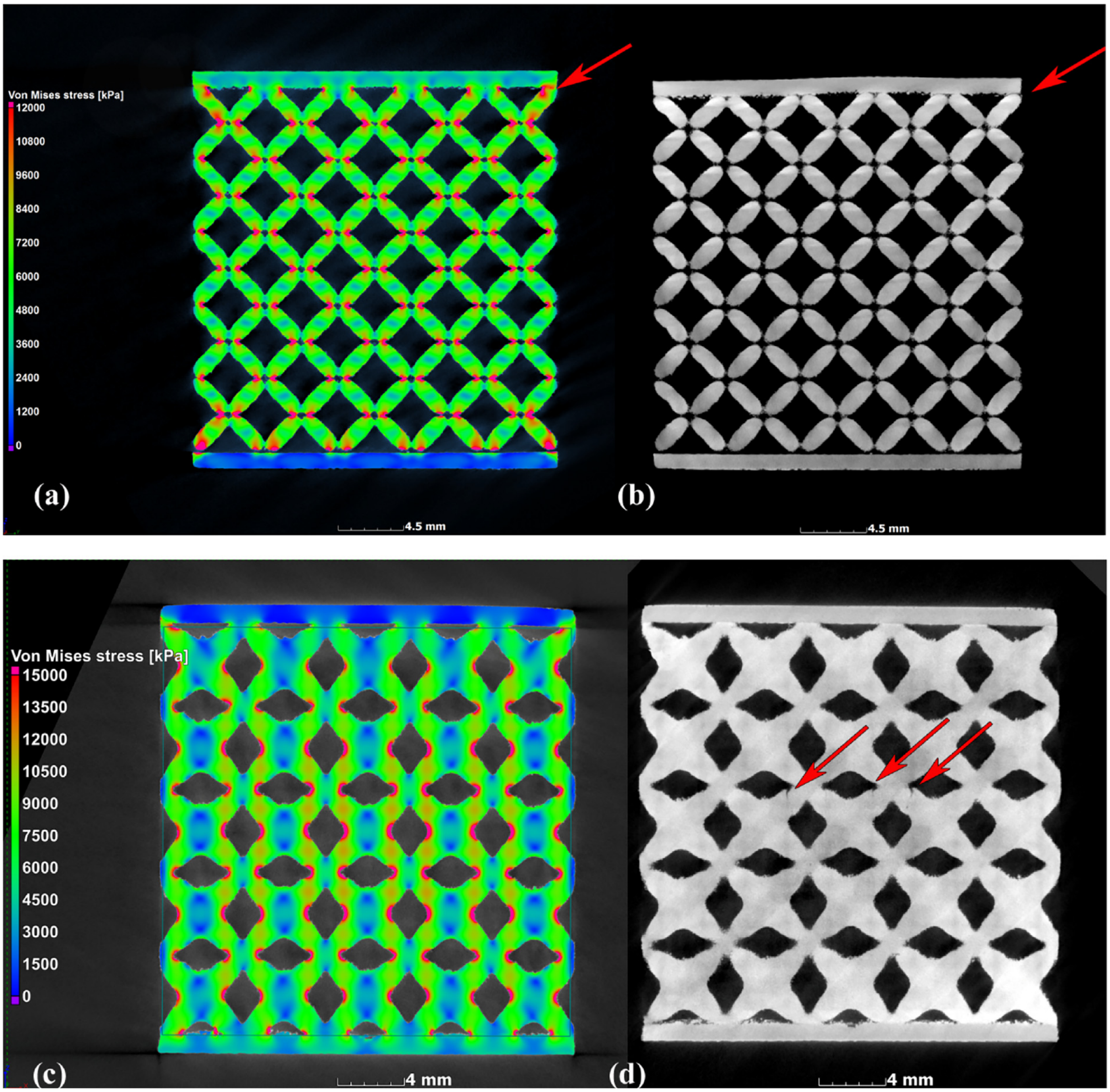

Fig. 7. Numerical simulation of von Mises stress (a, c) and orthogonal microCT slice images of the failure location (b, d). Failures are seen as thin black line/crack indicated with red arrows" (a,b) – rhombic and (c, d) – diagonal lattice structures. (For interpretation of the references to colour in this figure legend, the reader is referred to the web version of this article.)

the connection with the solid plate, this type of failure is not preferable. The mechanical test results confirmed simulation results: the rhombic design was found to have a lower maximal stress value in simulations, and in the mechanical tests it reached higher compressive stress before failure. However, both types had excellent ultimate compressive strength values. The Young's modulus values were variable but also confirmed simulation results.

4. Conclusions

We have demonstrated an analysis of rhombic and diagonal lattice structures, using voxel-based static load simulations to visualize and analyze von Mises stress distributions, applied advanced microCT morphological analysis and did physical compression testing of LPBF samples for which ultimate compressive strength and elastic modulus values could be obtained.

The simulations of microCT data compared to design ("*ideal*") data, indicate a significant increase in Von Mises stress in LPBF lattices compared to their design which can be attributed mainly to surface roughness and slightly reduced strut thickness. The simulations are validated by mechanical testing, providing values for the absolute compressive strength within a small range and effective compressive Young's modulus of the two structures.

In summary, we conclude that:

- By LPBF, both rhombic and diagonal designs were found to be produced with excellent reproducibility, free of defects and both were found to have high ultimate compressive stress values and effective compressive Young's modulus in the region expected, matching that of cortical bone.
- Load-bearing potential of these lattices are validated by mechanical tests, confirming first yielding only at ~ 120 kN for these 25 mm lattice samples.
- Stress simulations were conducted and large stress regions could be correlated with initial failure locations in both types of samples.

These lattice designs can therefore be confidently used in load-bearing applications in medical and other applications. The results are also promising for improving designs of lattice structures, and especially the stress hotspots found from simulations can be further used as inputs to designing customized stronger lattices by optimization of the thickness and shape of high-stress areas.

Acknowledgments

This work is based on the research supported by the South African Research Chairs Initiative of the Department of Science and Technology and National Research Foundation of South Africa (Grant № 97994) and the Collaborative Program in Additive Manufacturing (Contract № CSIR-NLC-CPAM-15-MOA-CUT-01). Samples were built in CRPM at Central University of Technology and authors would like to thank Mr. Johan Els. Mechanical testing has been performed in the mechanical testing laboratory of the Stellenbosch University and the authors are grateful to Mr. Lucas Anderson and Prof. Deborah Blaine.

Appendix A. Supplementary material

Supplementary data associated with this article can be found, in the online version, at https://doi.org/10.1016/j.optlastec.2018.07.050.

References

[1] M. Schmidt, M. Merklein, D. Bourell, D. Dimitrov, T. Hausotte, K. Wegener, L. Overmeyer, F. Vollertsen, G.N. Levy, Laser based additive manufacturing in industry and academia, CIRP Ann. Manuf. Techn. 66 (2017) 561–583.
[2] A.J. Pinkerton, Lasers in additive manufacturing, Opt. Laser Technol. 78 (2016) 25–32.
[3] D. Dai, D. Gu, H. Zhang, J. Xiong, C. Ma, C. Hong, R. Poprawe, R. IInfluence of scan strategy and molten pool configuration on microstructures and tensile properties of selective laser melting additive manufactured aluminum based parts, Opt. Laser Technol. 99 (2018) 91–100.
[4] L.E.J. Thomas-Seale, J.C. Kirkman-Brown, M.M. Attallah, D.M. Espino, D.E.T. Shepher, The barriers to the progression of additive manufacture: perspectives from UK industry, Int. J. Prod. Econ. 198 (2018) 104–118.
[5] L.E. Murr, K.N. Amato, S.J. Li, Y.X. Tian, X.Y. Cheng, S.M. Gaytan, E. Martinez, P. W. Shindo, F. Medina, R.B. Wicker, Microstructure and mechanical properties of open-cellular biomaterials prototypes for total knee replacement implants fabricated by electron beam melting, J. Mech. Behav. Biomed. Mater. 4 (2011) 1396–1411.
[6] C. Emmelmann, P. Sander, J. Kranz, E. Wycisk, Laser Additive Manufacturing and bionics: redefining lightweight design, Phys. Procedia 12 (2011) 364–368.
[7] M. Qian, D.L. Bourell, Additive manufacturing of titanium alloys, JOM 69 (2017) 2677–2678.
[8] L.J. Gibson, M.F. Ashby, Cellular Solids Structure and Properties, Cambridge University Press, Cambridge, 1997.
[9] S.E. Naleway, M.M. Porter, J. McKittrick, M.A. Meyers, Structural design elements in biological materials: application to bioinspiration, Adv. Mater. 27 (2015) 5455–5476.
[10] X.P. Tan, Y.J. Tan, C.S.L. Chow, S.B. Tor, W.Y. Yeong, Metallic powder-bed based 3D printing of cellular scaffolds for orthopaedic implants: A state-of-the-art review on manufacturing, topological design, mechanical properties and biocompatibility, Mater. Sci. Eng. C. 78 (2017) 1328–1343.
[11] X.Z. Shi, S.Y. Ma, C.M. Liu, Q.R. Wu, Parameter optimization for Ti-47Al-2Cr2Nb in selective laser melting based on geometric characteristics of single scan tracks, Opt. Laser Technol. 90 (2017) 71–79.
[12] B. Song, S.J. Dong, S.H. Deng, H.L. Liao, C. Coddet, Microstructure and tensile properties of iron parts fabricated by selective laser melting, Opt. Laser Technol. 56 (2014) 451–460.
[13] A. du Plessis, S.G. le Roux, S.G.A. Guelpa, The CT Scanner Facility at Stellenbosch University: An open access X-ray computed tomography laboratory, Nucl. Instrum. Methods. Phys. Res. B. 384 (2016) 42–49.
[14] A. du Plessis, S.G. le Roux, G. Booysen, J. Els, Quality control of a laser additive manufactured medical implant by X-ray tomography. 3D printing and additive, Manufacturing 3 (2016) 175–182.
[15] A. du Plessis, I. Yadroitsava, S.G. le Roux, I. Yadroitsev, J. Fieres, C. Reinhart, P. Rossouw, Prediction of mechanical performance of Ti6Al4V cast alloy, J. Alloys Compd. 724 (2017) 267–274.
[16] C. Broeckhoven, A. du Plessis, C. Hui, Functional trade-off between strength and thermal capacity of dermal armor: insights from girdled lizards, J. Mech. Behav. Biomed. Mater. 74 (2017) 189–194.
[17] H.D. Carlton et al., Mapping local deformation behavior in single cell metal lattice structures, Acta Mater. 129 (May 2017) 239–250.
[18] T.B. Sercombe et al., Failure modes in high strength and stiffness to weight scaffolds produced by Selective Laser Melting, Mater. Des. 67 (Feb. 2015) 501–508.
[19] I. Yadroitsev, P. Krakhmalev, I. Yadroitsava, A. du Plessis, Qualification of Ti6Al4V ELI alloy produced by laser powder bed fusion for biomedical applications, JOM 70 (2018) 372–377.
[20] T. Hildebrand, P. Rüegsegger, A new method for the model-independent assessment of thickness in three-dimensional images, J. Microscopy 185 (1997) 67–75.
[21] B. Vrancken, L. Thijs, J.P. Kruth, J. van Humbeeck, Heat treatment of Ti6Al4V produced by Selective Laser Melting: microstructure and mechanical properties, J. Alloy Compd. 541 (12) (2012) 177–185.
[22] W. Xu, S. Sun, J.Q. Elambasseril, M. Liu, M. Brandt, M. Qian, Ti-6Al-4V additively manufactured by Selective Laser Melting with superior mechanical properties, JOM 67 (2015) (2015) 668–673.
[23] S.J. Li, Q.S. Xu, Z. Wang, W.T. Hou, Y.T. Hao, R. Yang, L.E. Murr, Influence of cell shape on mechanical properties of Ti–6Al–4V meshes fabricated by electron beam melting method, Acta Biomater. 10 (2014) 4537–4547.
[24] Y. Choy, C.-N. Sun, K.-F. Leong, J. Wei, Compressive properties of Ti-6Al-4V lattice structures fabricated by selective laser melting: design, orientation and density, Add. Manuf. 16 (2017) 213–224.